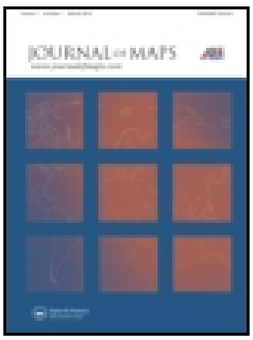

Journal of Maps

ISSN: (Print) (Online) Journal homepage: https://www.tandfonline.com/loi/tjom20

Geomorphology of the Central Kurdistan Region of Iraq: landscapes of the Erbil Plain between the Great Zab and Little Zab Rivers

Luca Forti, Andrea Pezzotta, Mjahid Zebari & Andrea Zerboni

To cite this article: Luca Forti, Andrea Pezzotta, Mjahid Zebari & Andrea Zerboni (2023): Geomorphology of the Central Kurdistan Region of Iraq: landscapes of the Erbil Plain between the Great Zab and Little Zab Rivers, Journal of Maps, DOI: 10.1080/17445647.2022.2164527

To link to this article: https://doi.org/10.1080/17445647.2022.2164527

JOURNAL OF MAPS
https://doi.org/10.1080/17445647.2022.2164527

SCIENCE

OPEN ACCESS Check for updates

Geomorphology of the Central Kurdistan Region of Iraq: landscapes of the Erbil Plain between the Great Zab and Little Zab Rivers

Luca Forti [a,b], Andrea Pezzotta [a], Mjahid Zebari [c] and Andrea Zerboni [a]

[a]Dipartimento di Scienze della Terra 'A. Desio', Università degli Studi di Milano, Milano, Italy; [b]Istituto di Geoscienze e Georisorse, CNR, Pisa, Italy; [c]Department of Earth and Environmental Sciences, Ludwig Maximilian University of Munich Luisenstr, Munich, Germany

ABSTRACT

We present the result of the geomorphological mapping of the central sector of the Kurdistan Region of Iraq. Therein, landscape evolution was mostly overseen by the regional geodynamic, related to the Arabia-Eurasia convergence, and in the Quaternary, regional climate fluctuations contributed to shaping landforms. The combination of such processes affected the distribution, types, and evolution of landforms (related to structural, hillslope, fluvial, and karst processes), with a noteworthy influence on the development of the local drainage network, which belongs to Tigris River catchment. The Great Zab and Little Zab Rivers – the main left tributaries of Tigris River – progressively cut anticline ridges growing in the area. Our analyses suggest that the structural deformation of the Zagros also controlled the evolution of the low-order channels of the hydrographic network. Since the Holocene, landforms dynamic was altered by intense human exploitation of the landscape and increased fluctuations between arid and humid conditions.

ARTICLE HISTORY
Received 21 June 2022
Revised 13 December 2022
Accepted 27 December 2022

KEYWORDS
Geomorphology; compressive tectonic; hydrographic network; Zagros Mountains; Kurdistan Region of Iraq

1. Introduction

The evolution, structure, and deformation of Earth's lithosphere play a huge influence on a variety of landforms of present-day landscapes (Burbank & Anderson, 2012). Among the many types of lithosphere dynamics, compressive tectonics can exhibit specific landforms (Owen & Shroder, 2013). In fact, along collisional mountain belt, compressive dynamic exerts a deep control over the evolution of hydrographic networks and related fluvial landforms; in such contexts, the trajectories of evolution of rivers result in different patterns depending on the structural settings of each region (Fryirs & Brierley, 2013; Trost et al., 2020). For instance, the central part of Kurdistan Region of Iraq (CKRI) represents a typical example of landscapes controlled by the compressive tectonic of the Zagros fold and thrust belt (ZFTB; Viltres et al., 2022) and shows a complex channel network (Forti et al., 2021; Forti et al., 2022). Its orientations and development are mainly related to the shortening of the ZFTB, evidencing that tectonic deformation acted as the main force on present and past geomorphic processes (Burbank & Anderson, 2012; Huggett, 2016). Moreover, river behavior is used as a control system to understand the deformations produced by lateral and frontal folds growth, usually associated with thrust activity (Bretis et al., 2011; Holbrook & Schumm, 1999; Jackson et al., 1998; Ramsey et al., 2008). In arid and semi-arid regions, water plays a key role in shaping the landscape and thanks to the poor plant cover their setting are evident in the field as much as from remote Earth observation (e.g. Costanzo et al., 2021; Perego et al., 2011). In such setting, fluvial landforms, and processes, as channel network, river dynamics, and characteristics (e.g. fluvial incision, basin drainage, and river avulsions), can be investigated to detect and quantify tectonic activity and subsurface structures (Obaid & Allen, 2017; Zebari et al., 2021). The combination of field and remote observation can also help in identifying the contribution of Quaternary climate fluctuations and how they affected the distribution and the amount of precipitation in the area. The latter, concurrently with the development of active tectonics, had a strong impact on alteration, erosion, transport, and deposition processes. The interplay between climate oscillations and tectonic forces is expressed in the present-day landscapes that characterize the CKRI (Forti et al., 2021; Fouad, 2015; Jassim & Goff, 2006; Zerboni et al., 2020).

In this work, we focus on the geomorphological analysis of the CKRI through the development of a regional geomorphological map (Main Map) aimed at reconstructing the Quaternary evolution of landforms and describing the influence on them of

CONTACT Luca Forti luca.forti@unimi.it; Andrea Pezzotta andrea.pezzotta@unimi.it Dipartimento di Scienze della Terra 'A. Desio', Università degli Studi di Milano, Milano 20122, Italy

Supplemental map for this article is available online at https://doi.org/10.1080/17445647.2022.2164527.

regional tectonic, which is likely the major factor controlling landscape evolution in the region, and climatic factors. We also report on active and inactive surface geomorphological processes and how they are controlled by endogenous and exogenous triggers, highlighting the role of compressive tectonic in shaping the hydrographic network. Moreover, we carefully consider the interplay between natural geomorphic processes and human activities because the region has been widely exploited by human communities since the Early Holocene, leaving their footprints over natural landforms.

2. Geographic, geological, and climatic backgrounds

The study area covers 12,000 km^2 within the CKRI encompassing the Governorates of Erbil, Niniveh, Kirkuk, and Sulaymaniyah. The main rivers are the Great Zab River (GZ) and the Little Zab River (LZ) that belong to into the Tigris River watershed. The high mountains within the ZFTB make the northeaster boundary of the Main Map, also these high mountains represent the principal orographic elements that characterize the landscape, reaching 2200 m asl. The mountain range is oriented NW-SE, and it is characterized by deep and incised canyons interspersed by with small plains. The connection between mountains and the flat area is transitional, through a foothills belt that reaches a maximum height of 1100 m asl. The flat areas, with minimum altitudes around 170 m asl along the main floor river valleys, are characterized by a fluvial network influenced by the ZFTB tectonic history and flowing alternatively in NW-SE and NE-SW directions. The Erbil Plain and the southern Kirkuk plain are the main alluvial areas. The ZFTB is a S-verging thrust and fold belt that is part of the Alpine-Himalayan orogenic system and comprises the KRI (Forti et al., 2021; Jassim & Goff, 2006). The ZFTB resulted from the convergence between Arabian and Eurasian plates, and subsequent continent-continent collision between the two plates during Oligocene that led to the closure of the Neotethys ocean (Koshnaw et al., 2020; Vergés et al., 2011; Zebari et al., 2019, 2020). The deformation propagated SW-ward on the NE passive margin of the Arabian Platform toward the Zagros Foreland Basin. The deformation is represented by the interplay between basement structures and fault-related folding of the sedimentary cover in which the lithological composition influenced the deformation style (Bretis et al., 2011; Koshnaw et al., 2020; Vergés et al., 2011: Zebari et al., 2020). The NW portion of the ZFTB can be divided into different morphotectonic zones, oriented NW-SE and separated by main faults. The study area is comprised between the High Folded Zone (HFZ), towards NE, and the Foothill Zone (FHZ), towards SW, separated by the Mountain Front Flexure (Jassim & Goff, 2006; Zebari et al., 2019, 2020). The Mountain Front Flexure is the main topographical and structural element that separates the HFZ, characterized by closely spaced (5–10 km wavelength) high anticlines, and the FHZ, showing widely spaced (up to 60 km wavelength) low anticlines and shallow synclines. The anticlines are mostly detachment-related or thrust-related (Zebari et al., 2020). The bedrock, composed by different sedimentary rocks, shows a rejuvenation in rock age from NE toward SW. Mesozoic-Paleogene sequence mainly consists of carbonates, while Neogene-Quaternary succession tends to be mainly siliciclastic (Sissakian & Al-Jibouri, 2012, 2014; Sissakian & Fouad, 2015). Quaternary deposits essentially consist of different continental terrigenous sediments covering small basins and infilling synclinal valleys especially in the FHZ (Sissakian & Al-Jibouri, 2012, 2014; Zebari et al., 2021). The climate of the study area is principally semi-arid, continental, sub-tropical type with an average annual rainfall of 428 mm and temperatures ranging from 7.8°C to 34.2° C (Rivas-Martìnez, 2004; Sissakian et al., 2014; Yacoub et al., 2012). Finally, the regions have been settled by human communities since the prehistory and local natural resources continuously exploited that have been investigated by several research projects (e.g. Peyronel et al., 2019; Ur et al., 2021). Human exploitation of the CKRI left a variety of anthropogenic landforms still evident in the field, such as the ancient citadels of Erbil and Kirkuk, the many tells dispersed along the Erbil Plain, and canal systems (Forti et al., 2021).

3. Methods

Geomorphological mapping of semi-arid and arid regions can be performed through a consolidated methodology that combines Earth observation techniques and field works (Azzoni et al., 2017, 2022; Costanzo et al., 2021; Forti et al., 2021; Hüneburg et al., 2019; Perego et al., 2011; Zerboni et al., 2015, 2020), and has been applied to the study area. Different datasets were retrieved and analyzed through remote sensing; all data has been reprojected to WGS 84 – UTM Zone 38N reference system within QGIS 3.16 and 3.20 software (QGIS Development Team, 2021). Recent high-resolution satellite imagery (2013–2021) was analyzed and visualized through 'QuickMapServices' plugin (NextGis, 2021). Furthermore, declassified CORONA intelligence satellite imagery (USGS, 1968), collected between 1967 and 1968 was utilized to recognize variations of landforms through historical time scales (Forti et al., 2022). Simultaneously, two digital terrain models (DTM) were used to evaluate and observe landforms: (i) Digital Surface Model (DSM) AW3D30 with horizontal resolution of 1 arcsecond (circa 30 m at the equator; JAXA, 2021); (ii) Digital Elevation Model (DEM) MERIT, with horizontal resolution of 3 arcseconds (circa 90 m at the equator; Yamazaki et al., 2017). These digital models

were reprojected with a spatial resolution of 30 m for DSM AW3D30 and of 90 m for DEM MERIT. Contour lines at 5, 10 and 100 m were extracted from digital terrain models and used for the landform interpretations, respectively, at 5 and 10 m for alluvial plain and detailed scale landforms, and at 100 m for highlands and general scale morphologies. In addition, elevation-dependent color scale, hillshade and slope models were derived from the DTMs through GRASS 7.8.3 and 7.8.5 (GRASS Development Team, 2020); these products were imported in QGIS and superimposed to observe different landforms (like river terraces, alluvial fans, wind, and water gaps) and to make comparisons with satellite imagery (Forti et al., 2021). The Quadrangles of the Series of geological Map of Iraq (1:250,000) of Arbeel-Mahabad, Al-Mosul, Kirkuk, and Sulaimanyia, compared with Geological Map of Iraq (1:1,000,000) have been digitalized and analyzed to identify bedrock chronology, lithologies, and structural elements (Maàla, 2008; Sissakian, 2013; Sissakian & Fouad, 2015, 2014) helpful in landscape reconstruction. The channel network was derived from Natural Earth (naturalearthdata.com), partially modified through comparison with satellite imagery and channel network extracted with GRASS. Field surveys validated geomorphological landforms and elements recognized through remote sensing analysis.

The channel network was also derived from DEM MERIT (Yamazaki et al., 2017) through GRASS software, and was processed to obtain a Strahler's hierarchical classification vector layer (Strahler, 1958). Analyses between channel segments and structural elements (faults and folds, mapped on the basis of Quadrangles of the Series of geological Map of Iraq) were illustrated through rose diagrams, extracted with the 'Line Direction Histogram' QGIS plugin (version 3.1.1; Tveite, 2015). Analyses of channel network orientations

Table 1. Nomenclature of the anticlines and synclines in the study area transliterated from the Arabic and Kurdish. Arabic names are from Maàla (2008), Sissakian (2013), and Sissakian and Fouad (2014). Kurdish names are from Shamaran petroleum (2011), Kurdistan Oil Resources (2013), and Koshnaw et al. (2020).

	Iraqi anticlines-synclines nomenclature	Kurdish anticlines-synclines nomenclature
High folded zone (HFZ)	Korak	Kurak
	Hareer	Harir
	Pelewan	Pelewan
	Kamosk	Kamosk
	Mirawa	Mirawa
	Shak Rook	Shakrok
	Shaqlawa	Seqlawa
	Khalikan	Khalakan
	Saafen	Safeen
	Permam	Pirmam
	Bana Bawi	Bina Bawi
	Maila	Maila
Foothill zone (FHZ)	Kewee Shirnella	Kewee Shirnella
	Taq Taq	Taq Taq
	Cham Chamal	Chemchemal
	Erbil	Erbil
	Dameer Dagh	Demir Dagh
	Khormala Dome	Khurmala Dome
	Guwair	Guwair
	Bai Hassan	Bai-Hasan
	Qara Chough	Qara Chug
	Qara Botak	Qara Botak
	Kirkuk	Kirkuk
	Taqultu	Taqultu
	Khal Kalan	Khalakan

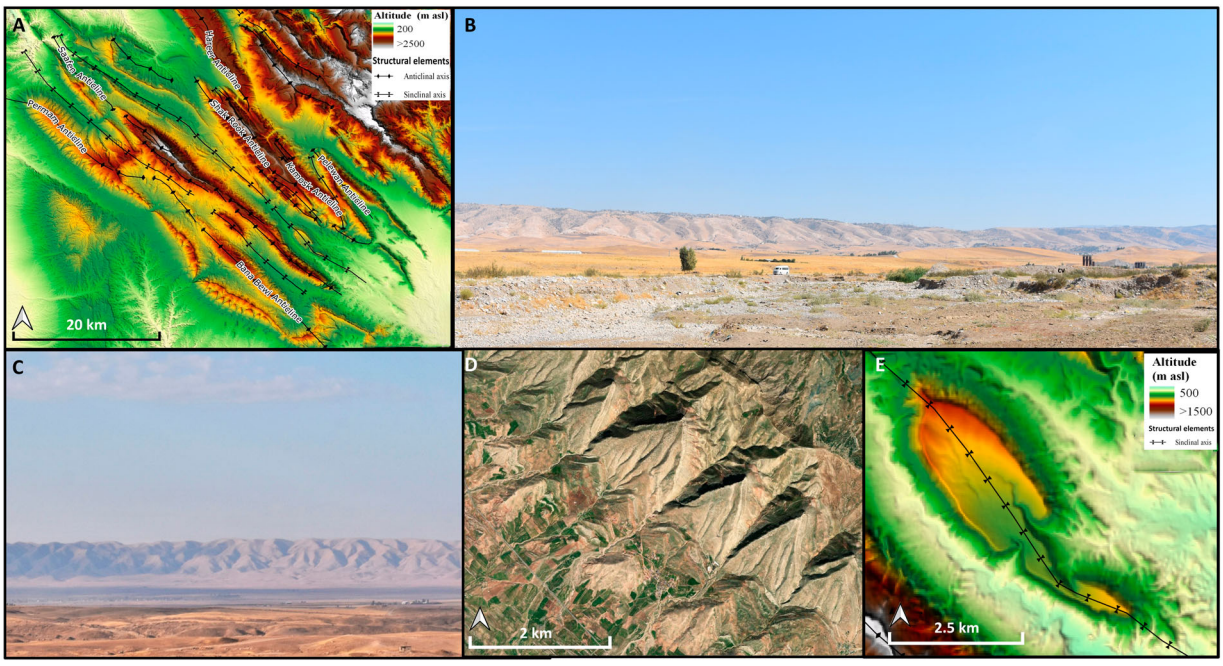

Figure 1. (A) DEM illustrating the orientation of the main anticlines and synclines in HFZ. (B) Western slope of the Permam Anticline. (C) Eastern limb of the Qara Choug Anticline crossed by several streams. (D) Esri satellite imagery showing the southern edge of the Bana Bewi Anticline marked by flatirons. (E) DEM of the syncline ridge valley located in the southern edge of the Saafen and Shak Rook Anticlines, resulting after differential erosion of sandstone (core) and limestone (forelimbs) strata.

considered both the totality of drainage segments and subdivided in each Strahler order. Histograms support comparison between the orientation of the channel network and major structural linear elements and allow validating hypothesis to explain the preferred orientation changes of channels according to the hierarchical order (e.g. Castiglioni, 1991; Kober et al., 2015; Obaid & Allen, 2017, 2019).

4. Main geomorphological features

4.1. Structural landforms

The development of mountain ridges and valley troughs and their orientations and morphologies are surface expression of the structures in the ZFTB orogen and pre-existing basement configuration (Obaid & Allen, 2017, 2019; Zebari et al., 2019, 2020). In this area, ridges generally correspond to anticline culminations, whereas valleys are the core of synclines (Figure 1(A)) additionally, there are anticlinal valleys where the core of anticline is deeply eroded and older rock units expose leaving both limbs as standing ridges. In some cases, triangular facets (flatirons) and wine glass forms are present in the limbs of anticlines, such as in the Qara Chough anticline (Figure 1(A)–5(D)). The study area includes the HFZ and FHZ that display different shortening rates and structural orientations (Fouad, 2015; Jassim & Goff, 2006; Zebari et al., 2019, 2020). Anticlines in the HFZ (from NW to SE are Korak, Hareer, Pelewan, Kamosk, Mirawa, Shak Rook, Khalikan, Saafen, Permam, Bana Bawi, and Maila anticlines; see Table 1 for comparisons between Iraqi and Kurdish nomenclature given the literature) are mainly oriented NW-SE to the east of the GZ and oriented nearly E-W to the west of the FZ. These anticlines are separated by narrow and deep synclinal valleys (Figure 1(A,B)). Lateral extension and linkage between adjacent anticlines are influenced by NE-SW trending transversal basement faults, and pre-existing normal faults that were formed during the Paleozoic extension and on the Mesozoic Arabian passive margin in Mesozoic time (Csontos et al., 2022; Zebari et al., 2020). These anticlines consist of Mesozoic-Paleogenic carbonates at the core and less competent Paleogene-Neogene terrigenous formations along the limbs and show a broad box geometry (Forti et al., 2021; Sissakian & Al-Jibouri, 2014; Zebari et al., 2019, 2021). Instead, anticlines in the FHZ (from NW to SE are Kewee Shirnella, Taq Taq, Cham Chamal, Erbil, Dameer Dagh East and West, Guwair, Bai Hassan, Northern and Southern Qara Chough, Qara Botak 1 and 2, and the ones associated with Kirkuk Thrust, as the Khormala Dome; see Table 1 for comparisons between Iraqi and Kurdish nomenclature given the literature) show NW-SE orientations (Figure 1(C)). Compared to the ones from the HFZ, they are widely spaced and display lower elevations; this is due to relatively lower deformation intensity in the HFZ in which only less competent lithological compositions of foreland basin are exposed, often characterized by Miocene-Pliocene marls, claystones, sandstones, and conglomerates that are more erodible than the Mesozoic-Paleogenic carbonates exposed the HFZ. In the FHZ, only the Qara Chough anticline show higher elevation a result of higher shortening and its steeper limb (Fouad, 2015; Le Garzic et al., 2019; Sissakian et al., 2018). Furthermore, anticlines in the FHZ

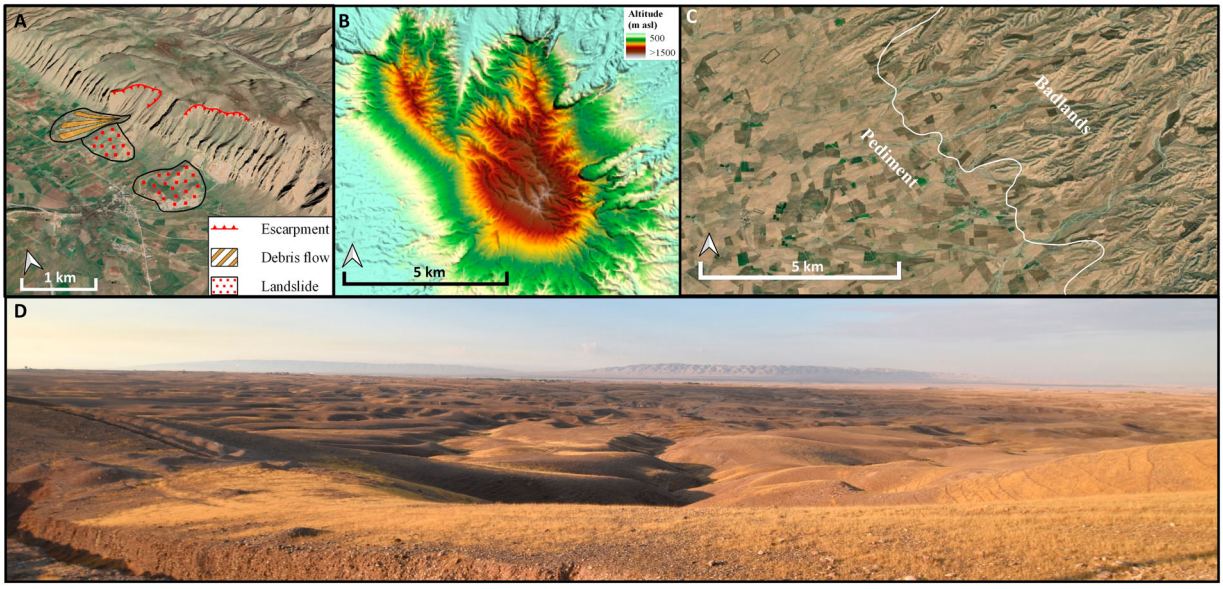

Figure 2. (A) Slope instability along the southern flank of the Hareer Anticline (sketch on GoogleEarth™ 3D imagery, 2× vertical exaggeration). (B) Badlands landscape north of Kirkuk extrapolated from DEM. (C) A pediment gently connected to the badland landscape north of Kirkuk (the white line indicated the boundary) (Esri World Imagery). (D) Western hillslope of the Khormala Anticline with a gently sloping pediment deep incised by gullies. In the background the Qara Chough anticline.

show major changes in the orientation of fold axis, corresponding to an en-echelon system, caused by differential uplift of each anticline. In this area, the anticlines are mostly fault related (Bretis et al., 2011). Wide synclines (Taqultu and Khal Khalan) are hanging synclines, filled by Quaternary fluvial, slope, and polygenetic sediments (Obaid & Allen, 2017, 2019; Sissakian, 2013; Sissakian & Fouad, 2014; Zebari et al., 2020, 2021).

Along their slopes and limbs, folds often show monocline motives, including cuestas and hogbacks slope reliefs. In the Main Map, cuestas and hogbacks are not differentiated because the exposure of satellite images prevents their certain attribution to one of the two categories. Yet, flatirons belts were mapped to evidence forelimbs and toe of anticlines that show slope triangular shapes (Forti et al., 2021) (Figure 1(D)). The Shaqlawa Syncline valley, located in the southern edge of the Saafen and Shak Rook anticline and influenced by a thrust fault (Le Garzic et al., 2019; Sissakian et al., 2021), is an example of inverted relief; in fact, erosion was more efficient along the soft sandstone Paleocene-Eocene core than along the Cretaceous carbonate limbs (Figure 1(E)).

4.2. Hillslope and gravitative landforms

Apart of being cut into flatirons, the hillslope of anticlines in the HFZ and FHZ are affected by different processes related to gravity, seasonal climate variability, bedrock type, weathering amount, erosional and transport capacities (Forti et al., 2021; Sissakian et al., 2020). Sissakian et al. (2020) report that several localities along the LZ are affected by hillslope gravitative processes (e.g. landslide, mudflow and rockfalls) that influenced the river dynamics. Most of landslides are small and not suitable to be represented at the scale of the Main Map. A few large landslides are included

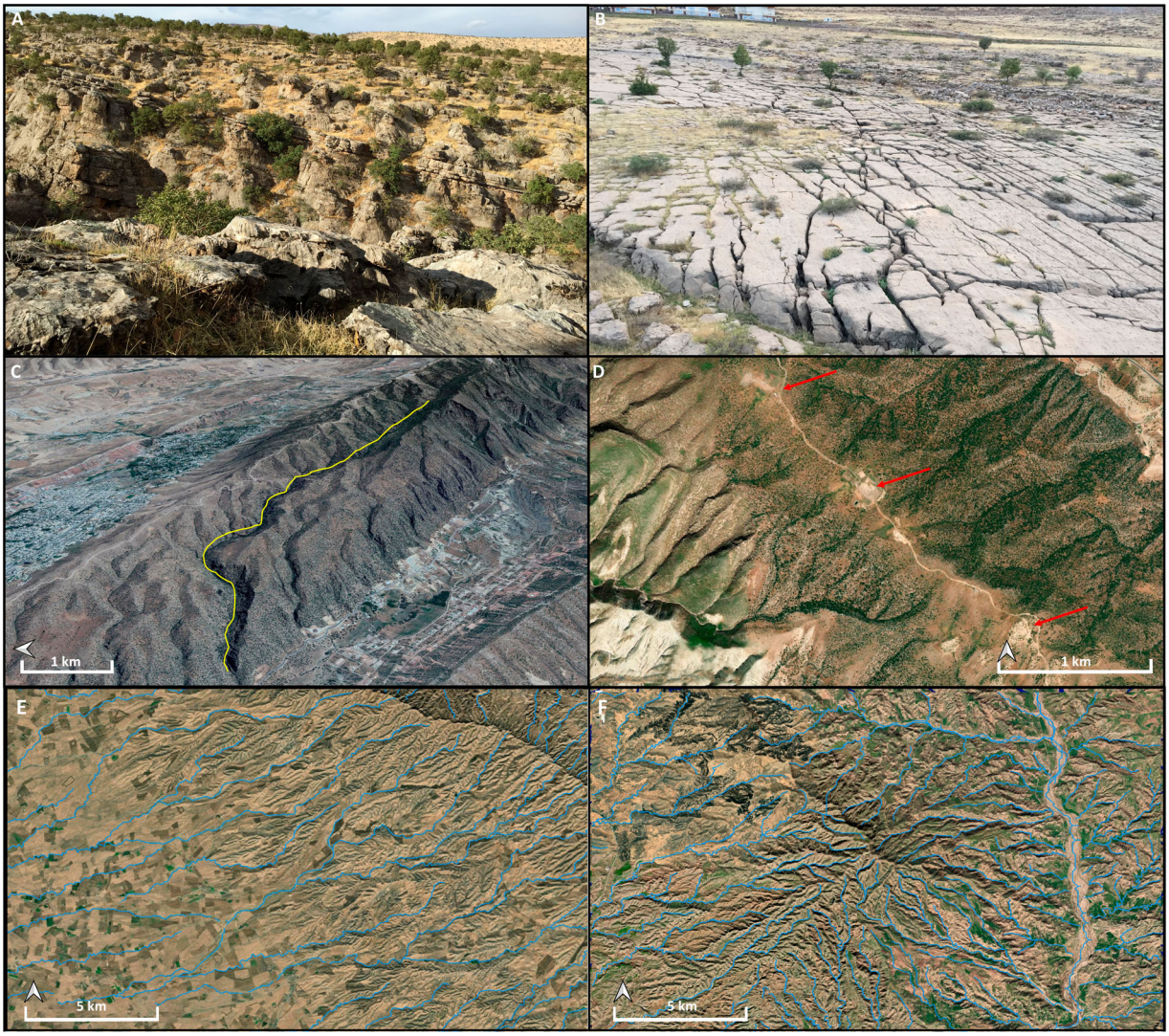

Figure 3. (A) Limestone landscape with epikarst landforms. (B) Slope anticline of Karak anticline characterized by limestone pavement. (C) Stephead valley (red line) in the northern sector of the Saafen Anticline resulted by the interaction between karst and fluvial processes (Google Earth™ 3D imagery, 2× vertical exaggeration). (D) Dolines at the top of the Bana Bewi anticline (red arrows). Different types of drainage pattern driven by the geological and structural setting of the study area: (E) dendritic and (D) radial settings.

in the Main Map, and they are located along the slopes of Hareer and Maila anticlines and on the ridges at the left bank of GZ (Figure 2(A)). Monocline slopes E and SE of Erbil and N of Kirkuk consist of terrigenous lithologies and are widely dissected by rills and gullies networks, resulting in a badland landscape (Figure 2 (B)). The connection between erosional slopes and plains is characterized by a gently pediment incised by seasonal rills and gullies networks and today exploited for cultivation (Figure 2(C,D)).

4.3. Karst landforms

Limestone ridges are affected by dissolution processes resulting into a karst landscape including epikarst and ipokarst landforms (Figure 3(A)). Major caves are not known in the study area, but several caves and rock shelters open in nearby areas of the Zagros, resulting from hypogenic and epigenic processes (Forti et al., 2021; Laumanns et al., 2008). On top of the ridges, limestone pavements are evident with small to medium-scale epikarst features (Figure 3(B)). Moreover, several deeply incised gorges and canyons are likely the result of interplay between geological setting, fluvial and karst processes; among the others, gorges cut the Saafen, Bana Bewi, Pelewan, Hareer, and Permam anticlines (Figure 3(C)). Several dolines are located at the top of anticlines of Permam and Bana Bewi (Figure 3(D)).

4.4. Fluvial landforms

The fluvial landscape of the CKRI is modeled along the catchments of the GZ and LZ rivers. Therein, the

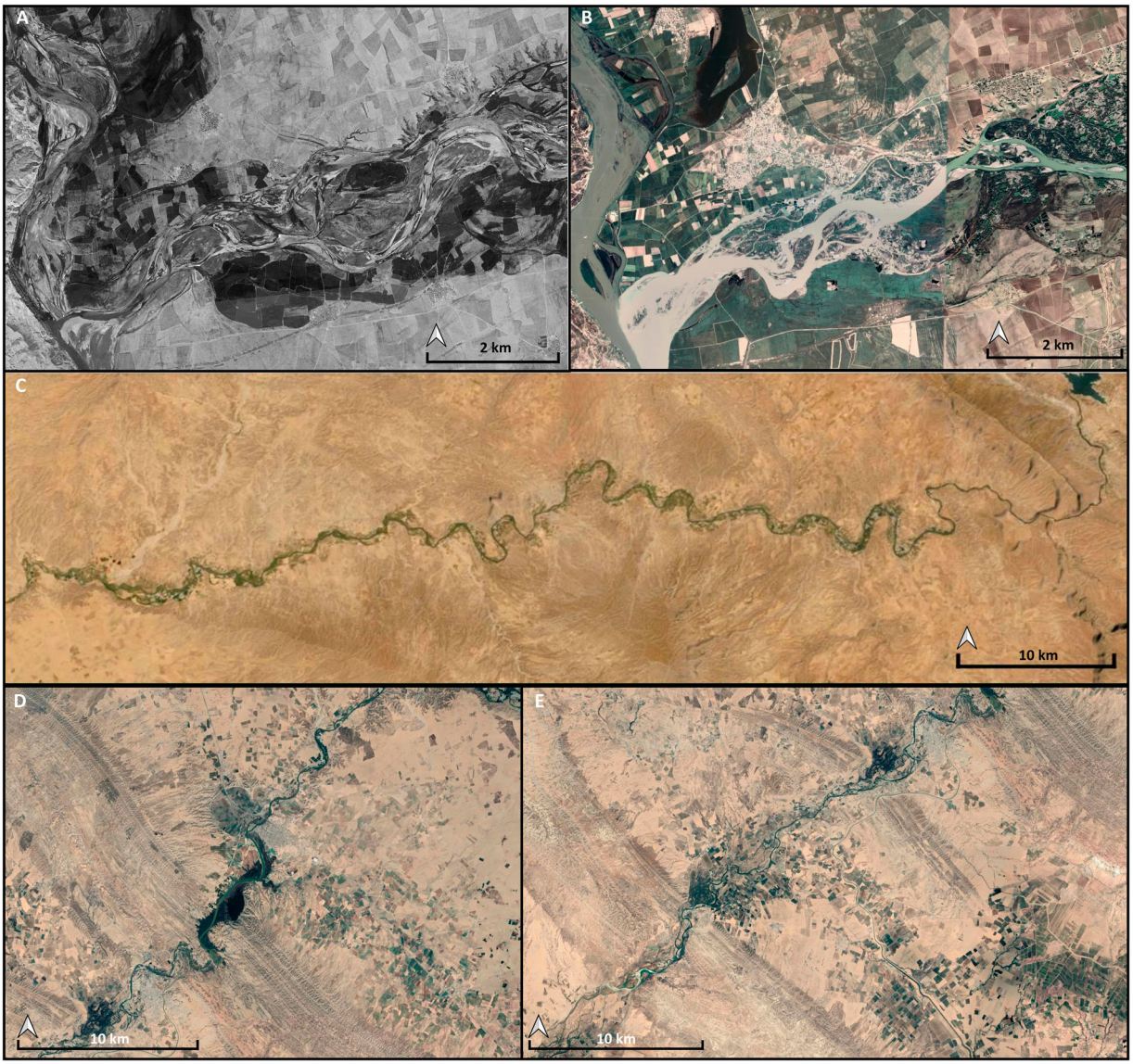

Figure 4. The anabranching planform of the GZ River before its conjunction with the Tigris River from (A) declassified Corona Imagery (August 1968) and (B) Google Earth™ satellite imagery (captured in January 2019). (C) Upstream reach of the LS River that flows with a E-W trend and displays a decrease in meanders sinuosity (Esri Satellite). (D) Downstream reach of LZ before in the NE of Kirkuk city, where the river switch toward NE-SW (Google Earth™ satellite imagery). (E) Downstream reach of LZ in the NE of Kirkuk city, with development of floodplain (Google Earth™ satellite imagery).

direction and plan geometry of fluvial networks is related to (i) the orientation of anticline and syncline systems and regional faults, (ii) slope gradient, (iii) lithology of the bedrock, and (iv) landslides (Fryirs & Brierley, 2013; Obaid & Allen, 2017, 2019; Sissakian et al., 2020; Tooth et al., 2014; Zebari et al., 2021). Such factors influenced the evolution of a differentiated fluvial pattern. In fact, in the mountainous area of HFZ the network is dendritic, with a NW-SE preferential orientation that follows the direction of syncline valleys; on the contrary, in the FHZ streams have a NE-SW to NW-SE direction and display a dendritic to radial drainage setting (Figure 3(E,F)). Considering the two major rivers, the GZ follows a NE-SW orientation, locally shifting WSW-ENE in the proximity of the Guwair anticline. In the area between the upstream to its connection with the Tigris River, the GZ River has a single thread with a low sinuosity degree of meandering and irregular meanders pattern. Before merging into the Tigris River, the course of the GZ River shifts to an anabranching channel planform with up to three seasonal channels (Figure 4(A,B)). The LZ River follows a general ENE-WSW trend with a change toward NE-SW sectors 15 km before the Altun Kupri town. In its upstream sector, located between the HFZ and NE of FHZ, different lithotypes and landslides oversee the fluvial dynamic of the LZ River (Figure 4(C)). Between the Goptapa village and the Taq Taq anticline, the LZ River crosses conglomerates and sandstones displaying a single tortuous to irregular meandering thread pattern. From the Taq Taq anticline to Altun Kupri the course of the LZ becomes straight, displaying a channel with a low sinuosity and irregular meandering pattern. The final reach of the LZ River – in the FHZ – shows a low sinuosity with irregular meanders close to the Kirkuk anticline with a progressive increase in the degree and type of sinuosity before the Qara Botak anticline (Figure 4(D,E)). This is

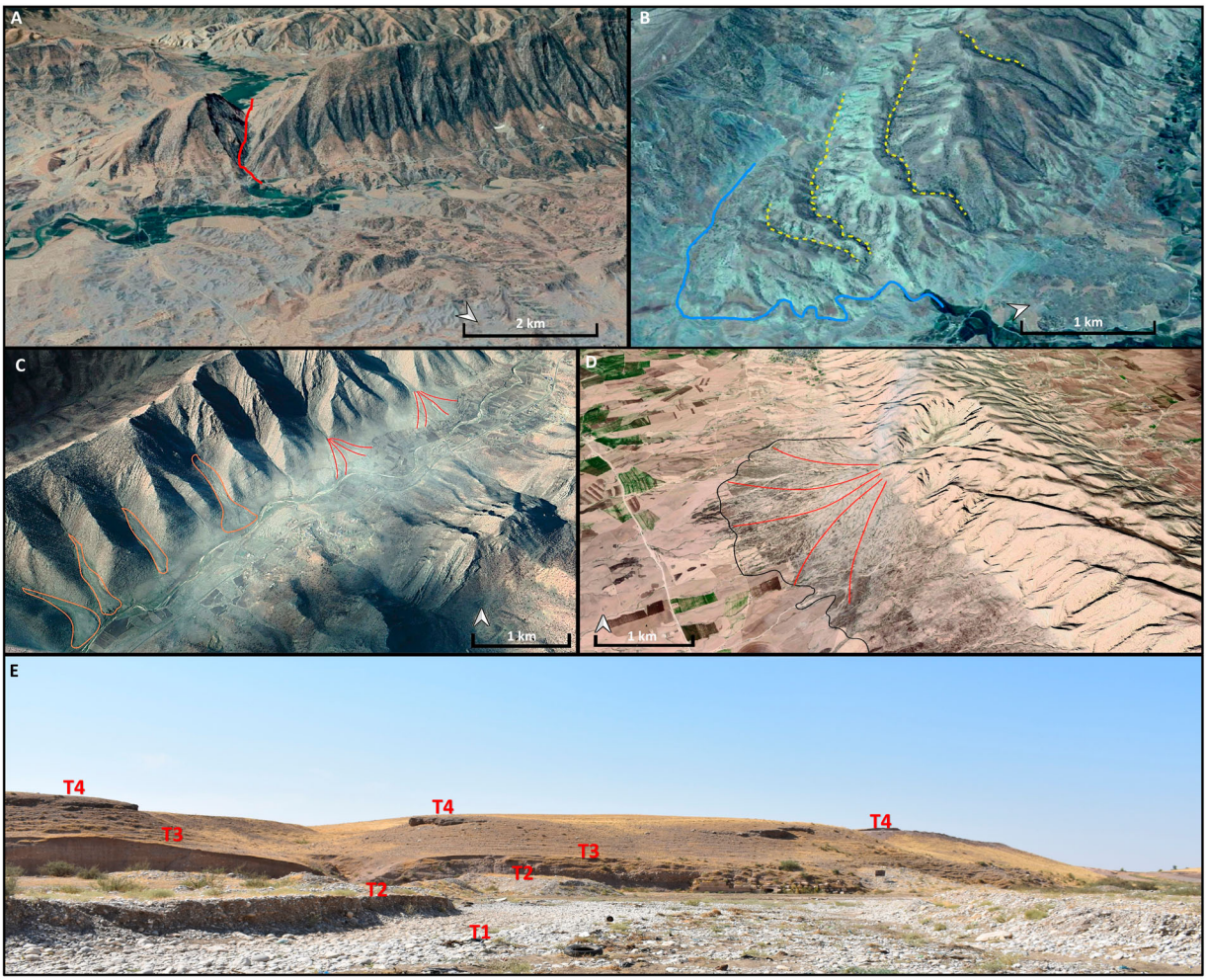

Figure 5. Water gap in SE sector of Saafen anticline (elaborated from Google Earth™ D imagery, 2× vertical exaggeration). (B) Southern edge of the Bana Bewi Anticline showing four wind gaps (yellow dotted lines) and the active river course (blue line) (elaborated from Google Earth™ D imagery, 2× vertical exaggeration). (C) Google Earth™ 3D imagery (3× vertical exaggeration) of the eastern limb of the Pelewan anticline dissected by several V-shape valleys (wineglass landform) with debris flow fans (orange polygons) and outlet alluvial fans (red lines). (D) Alluvial fan (red lines) and bajada envelope (black line) along the western limb of the Qara Chough anticline (elaborated on Google Earth™ 3D imagery, 2× vertical exaggeration). (E) Terraced banks of the Chai Basturah River, NE of Erbil; the order of terraces is reported.

triggered by the decrease in the slope gradient and growth of anticlines. Sissakian et al. (2020) suggest that the pattern of different portions of the extant shape of LZ is influenced by the activation of landslides (Taq Taq, Bul-Qamish, and Saralu landslides) which modify the meandering and the general plan geometry of LZ. Today, water gap gorges are the main waterways connecting the HFZ highland with FHZ lowland (Figure 5(A)). The main water gap gorges are 500 m to 50 m deep and developed into the Hareer, Saafen, Khalikan, and Bana Bewi anticlines in the HFZ. Several wind gaps dry valley cut the southern sector of the Bana Bewi anticline (Figure 5 (B)). Along the LZ watercourse from upstream to downstream, several water gap gorges developed into the anticlines of Maila, Taq Taq, Chamchamal, Kirkuk Structure, Bai Hassan, and Qara Botak. The slopes of HFZ ridges are carved by streams forming series of wineglass landforms and by deep V-shaped valleys, resulting into deep gorges. Unconsolidated materials characterized the valley floor of these gorges in which at termination we notice the presence of debris flow and alluvial fans, the oldest are covered by a thick calcrete, locally dissected by sheet erosion (Sissakian et al., 2015) (Figure 5(C)). Anticlines' slopes in the LFZ are dissected by streams that build outlet of the valleys several coalescing alluvial fans forming a bajada feature (Figure 5(D)).

Lowlands are characterized by wide floodplains located in the surrounding Erbil and Kirkuk. Floodplains mainly consist of reddish silty-clay deposits interbedded with coarser layers and it is dissected into four orders of fluvial terraces; the main river courses display a gravel-dominated to silty bed. The younger terraces (T1, T2, and T3) formed in the Late Quaternary and are composed by pebble and cobble in a sandy matrix with interlayered medium to coarse sand, while the oldest terrace (T4) consists of Plio-Pleistocene conglomerates (Dokan conglomerate in the upperstream portion of the LZ) (Figure 5(E)) (Sissakian & Fouad, 2015). In the NW sector of the study area, some of the GZ fluvial terraces are tilted by Quaternary neotectonics (Zebari et al., 2021).

4.5. Anthropogenic landforms

Since the Early and Middle Holocene, the natural landscape of the CKRI has been strongly affected by human activities, including cultivation, herding,

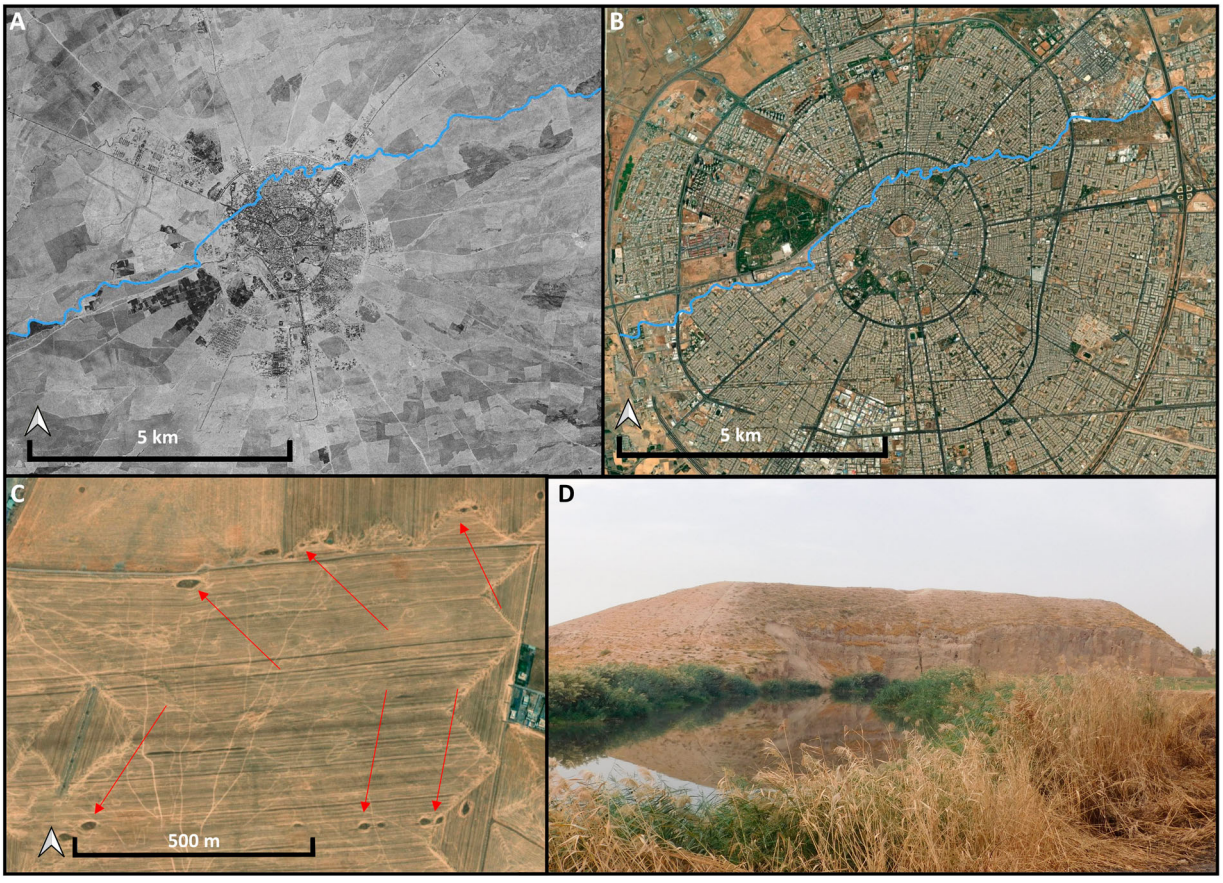

Figure 6. Anthropogenic landforms in the study area. Comparison between (A) 1968 Declassified Corona and (B) Esri World view imagery (captured in November 2020) that show the intense urban expansion of Erbil; the blue line indicates a former fluvial channel recently forced underground with consequence hydrographic network modification. (C) Qanat alignment in the proximity of Erbil (red arrows) (Bing Virtual Earth). (D) Archeological mound (tell) in the Erbil Plain (Tell Awena).

and water management in the region. Consequently, several anthropogenic landforms are the result of an intense land exploitation that started in the prehistory and recently exacerbated by exponential growth of urban centers (Figure 6(A,B)). In the Late Holocene, the progressively increasing demand for primary resources (such as water) and enhanced aridity promoted the introduction of extensive implements for water management; for instance, the underground qanat (Karez) system (Figure 6 (C)) for water harvesting from the alluvial fans was introduced several centuries ago (Soroush et al., 2020). Moreover, several dams, water reservoirs, and artificial canals were recently built to support intensive cultivation. Modern facilities for water management are located mostly in the proximity of Erbil and Kirkuk, notably along the GZ and LZ Rivers and at the foothills of anticline ridges. A large artificial canal excavated S of Kirkuk connects the LZ with the southern Adhaim and Diyala plains. Dams and related water reservoirs are in the sector N of Kirkuk and SE of the Bana Bewi anticline.

Several archeological mounds arise from the surrounding flat areas; they are tell sites and were formed by the accumulation of human sediments after millennia of occupation (Miller Rosen, 1986; Wilkinson, 2003) (Figure 6(D)). Such anthropogenic landforms testify for the long-term exploitation of CKRI. Tells are common in the floodplain S of Erbil (Peyronel et al., 2019; Ur et al., 2021), and they are generally located along active/ephemeral meandering streams or paleochannels.

5. Hydro-morphometric analysis: tectonic influence on channel network organization

The effects of differential uplift, linked to Neogene-recent tectonic activity, can be recognized also through the analyses of different fluvial patterns and river variation. In fact, in tectonically dynamic areas rivers tend to set up their directions based on structural elements (e.g. Kober et al., 2015; Obaid & Allen, 2017, 2019; Siravo et al., 2021; Trost et al., 2020; Woolderink et al., 2021). Our analyses of fluvial network (summarized in Figure 7) illustrate that the rose diagram of the 1st order of stream segments has a NE-SW preferential orientation, perpendicular to the trend of structural elements (anticlines and faults). This reflects the tendency of the minimum hierarchical tracts to set along the direction of maximum slope gradient. The second order of stream segments shows a preferential trend directed NE-SW, but there is a significant NW-SE and E-W component. In this case, directional variability is ruled out by the interplay between: (i) the NE-SW preferential trend is influenced by direction of maximum slope gradient, (ii) the NW-SE alignment corresponds to the trend of folds and faults, (iii) E-W trend is determined

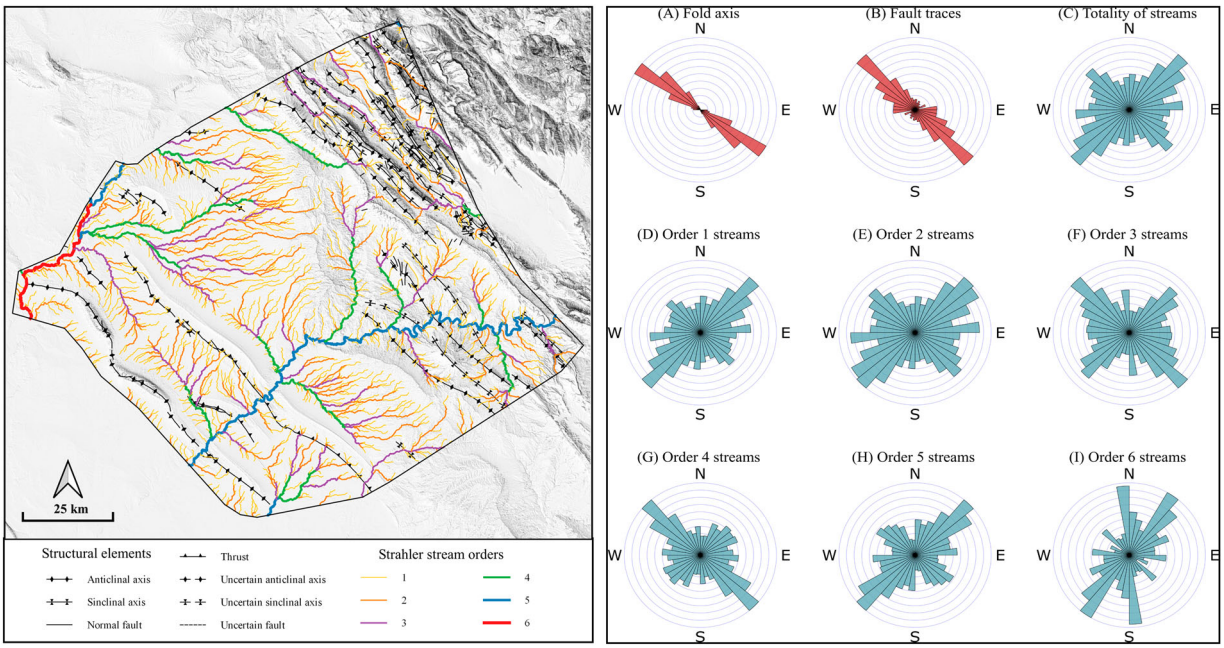

Figure 7. Grayscale Dem of the study area with the different structural and Strahler's stream orders Rose Diagram histograms. Rose diagrams are based on number of analyzed elements and on weight of length. The histograms show that structures (references for geological features see Methods) have a general NW-SE orientation, with a principal concentration for the fold axis, while fault traces have a broader distribution. Channel network's histograms are more complex. The histogram of all fluvial courses' marks three preferential orientations (in order, NE-SW, NW-SE, E-W). The rose diagrams of lower hierarchical Strahler's classes (order 1 and 2) show a NE-SW preferential orientation, perpendicular respect to structural elements trend. Order 3 and 4 stream segments have a NW-SE preferential orientation, parallel to structural elements direction. Histogram of order 5 waterways shows a NE-SW trend, while order 6 channels show a NE-SW preferential trend followed by a NNW-SSE orientation.

principally by hydrographic networks developed in the reliefs NE of the Erbil Plain. The third and fourth orders of stream segments show a NW-SE preferential orientation, responding to a major structural control; these segments run parallel to faults and synclinal valleys axis. They are responsible of the accretion of floodplains along synclinal valleys. Rose diagram of the fifth order of stream segments shows a NE-SW preferential orientation, but in this hierarchical class only includes some segments of the GZ and LZ Rivers. The latter align along basement strike-slip faults that dislocate tectonic blocks (Jassim & Goff, 2006). The sixth order of stream segments (corresponding to the Tigris River and last part of GZ River) shows a NE-SW preferential trend followed by a N-S orientation. The NE-SW direction is influenced by basement strike-slip faults, while NNW-SSE trend is also related to an inferred strike-slip fault located along the Tigris River course (Fouad, 2015; Jassim & Goff, 2006) (Figure 7).

6. Conclusion

Geomorphological mapping of the CKRI permitted to recognize different geomorphological units resulting from the many processes that shaped the landscape at the regional scale during the Late Cenozoic. Our investigation highlights the major influence of tectonic and climatic variations in modeling landforms. Compressive tectonic and Quaternary neotectonic led to the organization of the landscape into subsequent ridges and valleys corresponding to anticlines and synclines respectively; this also influenced the evolution of the channels network. Quaternary climate oscillations impacted on the variations in flow rate, amount of solid load and consequently on fluvial landforms. In the last millennia, anthropic impact has grown, which determined modifications of natural landscape and creation of anthropogenic landforms. The exploitation of natural resources has determined the transformation and continuous shaping of the territory, which have increased in parallel with the development of complex societies. In this scenario, overlapping of endogenous and exogenous factors has determined the formation of a palimpsest landscape, in which active and fossil stratified elements and processes can be recognized. Finally, geomorphological mapping of long-time settled landscapes – as the CKRI is – offers important tools for urban planning as much as a plethora of information to reconstruct past human adaptations, subsistence strategies, and early human overprints on pristine geomorphic systems.

Software

The project map and all shapefiles were realized using QGIS 3.16 and 3.20. Terrain analyses for DTMs and hydrographic network were carried out in GRASS 7.8.3 and 7.8.5. Specific observations from satellite images were done with Google Earth Pro 7.3.4.

Acknowledgments

This research was conducted under the umbrella of the Italian Archaeological Mission in the Erbil Plain of the Università degli Studi di Milano (MAIPE) (directed by Luca Peyronel and Agnese Vacca who are kindly acknowledged for their support). We are grateful to the General Directorate of Antiquities of the Kurdistan Regional Government, the Directorate of Antiquities of Erbil. Funding for analyses was provided by the Università degli Studi di Milano, Progetto Linea 2 (2017) and project CTE_NAZPR19AZERB_01 entrusted to A. Zerboni. Part of this research was supported by the Italian Ministry of Education, Universities, and Research (MIUR) through the project 'Dipartimenti di Eccellenza 2018–2022' (WP4 – Risorse del Patrimonio Culturale) awarded to the Dipartimento di Scienze della Terra 'A. Desio' of the Università degli Studi di Milano.

Disclosure statement

No potential conflict of interest was reported by the author(s).

Data availability statement

The Digital Surface Model (DSM) AW3D30 with horizontal resolution of 1 arcsecond used as basemap is free downloaded from https://www.eorc.jaxa.jp/ALOS/en/dataset/aw3d30/aw3d30_e.htm and Digital Elevation Model (DEM) MERIT, with horizontal resolution of 3 arcseconds for channel network analysis is free downloaded from http://hydro.iis.u-tokyo.ac.jp/~yamadai/MERIT_Hydro/. Corona Dataset were free downloaded from the site of University of Arkansas https://corona.cast.uark.edu/atlas#zoom=3&center=0,3000000. The data supporting of this study are available from the corresponding authors, upon reasonable request.

ORCID

Luca Forti http://orcid.org/0000-0002-2965-9955
Andrea Pezzotta http://orcid.org/0000-0002-1093-1576
Mjahid Zebari http://orcid.org/0000-0002-7292-8962
Andrea Zerboni http://orcid.org/0000-0002-6844-8528

References

Azzoni, R. S., Bollati, I. M., Pelfini, M., Sarıkaya, M. A., & Zerboni, A. (2022). Geomorphology of a recently deglaciated high mountain area in Eastern Anatolia (Turkey). *Journal of Maps*, *18*(2), 258–267. https://doi.org/10.1080/17445647.2022.2035269

Azzoni, R. S., Zerboni, A., Pelfini, M., Garzonio, C. A., Cioni, R., Meraldi, E., & Diolaiuti, G. A. (2017). Geomorphology of mount ararat/Ağri Dağı (Ağri Dağı milli parki, Eastern Anatolia, Turkey). *Journal of Maps*, *13*(2), 182–190. https://doi.org/10.1080/17445647.2017.1279084

Bretis, B., Bartl, N., & Grasemann, B. (2011). Lateral fold growth and linkage in the Zagros fold and thrust belt

(Kurdistan, NE Iraq). *Basin Research*, *23*(6), 615–630. https://doi.org/10.1111/j.1365-2117.2011.00506.x

Burbank, D. W., & Anderson, R. S. (2012). *Tectonic geomorphology* (p. 454). John Wiley and Sons.

Castiglioni, G. B. (1991). *Geomorfologia* (Seconda edizione, p. 436). UTET.

Costanzo, S., Zerboni, A., Cremaschi, M., & Manzo, A. (2021). Geomorphology and (palaeo-) hydrography of the Southern Atbai plain and western Eritrean Highlands (Eastern Sudan/Western Eritrea). *Journal of Maps*, *17*(2), 51–62. https://doi.org/10.1080/17445647.2020.1869112

Csontos, L., Forián Szabó, M., Pocsai, T., Magyari, A., & Soós, B. (2022). Fold formation in Kurdish Zagros (N Iraq). *Marine and Petroleum Geology*, 146, 105914. ISSN 0264-8172. https://doi.org/10.1016/j.marpetgeo.2022.105914

Forti, L., Mariani, G. S., Brandolini, F., Pezzotta, A., & Zerboni, A. (2022). Declassified intelligence satellite imagery as a tool to reconstruct past landforms and surface processes. The submerged riverscape of the Tigris River below the Mosul Dam Lake, Iraq. *Earth Surface Processes and Landforms*, *47*(10), 2483–2499. https://doi.org/10.1002/esp.5389

Forti, L., Perego, A., Brandolini, F., Mariani, G. S., Zebari, M., Nicoll, K., Regattieri, E., Conati Barbaro, C., Morandi Bonacossi, D., Qasim, H. A., Cremaschi, M., & Zerboni, A. (2021). Geomorphology of the northwestern Kurdistan Region of Iraq: landscapes of the Zagros Mountains drained by the Tigris and Great Zab Rivers. *Journal of Maps*, *17*(2), 225–236. https://doi.org/10.1080/17445647.2021.1906339

Fouad, S. (2015). Tectonic map of Iraq, scale 1:1000,000, 3rd edition. *Iraqi Bulletin of Geology and Mining*, *11*, 1–7.

Fryirs, K. A., & Brierley, G. J. (2013). *Geomorphic analysis of river systems. An approach to reading the landscape* (p. 345). Wiley-Blackwell.

GRASS Development Team. (2020). Geographic Resources Analysis Support System (GRASS) Software, Version 7.8. Open Source Geospatial Foundation. https://grass.osgeo.org

Holbrook, J., & Schumm, S. A. (1999). Geomorphic and sedimentary response of rivers to tectonic deformation: A brief review and critique of a tool for recognizing subtle epeirogenic deformation in modern and ancient settings. *Tectonophysics*, *305*(1–3), 287–306. https://doi.org/10.1016/S0040-1951(99)00011-6

Huggett, R. J. (2016). *Fundamentals of geomorphology*. Routledge.

Hüneburg, L., Hoelzmann, P., Knitter, D., Teichert, B., Richter, C., Lüthgens, C., Alsaud, A. S., & Luciani, M. (2019). Living at the wadi – Integrating geomorphology and archaeology at the oasis of Qurayyah (NW Arabia). *Journal of Maps*, *15*(2), 215–226. https://doi.org/10.1080/17445647.2019.1576068

Jackson, J., van Dissen, R., & Berryman, K. (1998). Tilting of active folds and faults in the Manawatu region, New Zealand: Evidence from surface drainage patterns. *New Zealand Journal of Geology and Geophysics*, *41*(4), 377–385. https://doi.org/10.1080/00288306.1998.9514817

Jassim, S. Z., & Goff, J. C. (2006). *Geology of Iraq* (p. 341). Dolin, Prague and Moravian Museum.

JAXA. (2021). ALOS Global Digital Surface Model 'ALOS World 3D – 30 m (AW3D30)'. Retrieved August 11, 2021, from https://www.eorc.jaxa.jp/ALOS/en/aw3d30/

Kober, F., Zeilinger, G., Hippe, K., Marc, O., Lendzioch, T., Grischott, R., Christl, M., Kubik, P. W., & Zola, R. (2015). Tectonic and lithological controls on denudation rates in the central Bolivian Andes. *Tectonophysics*, *657*, 230–244. ISSN 0040-1951. https://doi.org/10.1016/j.tecto.2015.06.037

Koshnaw, R. I., Stockli, D. F., Horton, B. K., Teixell, A., Barber, D. E., & Kendall, J. J. (2020). Late Miocene deformation kinematics along the NW Zagros fold-thrust belt, Kurdistan region of Iraq: Constraints from apatite (U-Th)/He thermochronometry and balanced cross sections. *Tectonics*, *39*(12), 12. https://doi.org/10.1029/2019TC005865

Kurdistan Oil Resources. (2013). Discoveries and Development. Wildcat International FZ-LLC. The Oil & Gas Year, Kurdistan Region of Iraq. http://archive.gov.krd/mnr/mnr.krg.org/images/pdfs/Discoveries_and_development_TOGY_2013_1.pdf

Laumanns, M., Rasch, A., & Audra, P. (2008). *Karst and Caves of Iraq (including the results of a 2007 Kurdish-German speleological project and an overview on hypogenic sulphidic speleogenesis)* (p. 26). Berliner Höhlenkundliche Berichte.

Le Garzic, E., Vergés, J., Sapin, F., Saura, E., Meresse, F., & Ringenbach, J. C. (2019). Evolution of the NW Zagros Fold-and-Thrust Belt in Kurdistan Region of Iraq from balanced and restored crustal-scale sections and forward modeling. *Journal of Structural Geology*, *124*, 51–69. https://doi.org/10.1016/j.jsg.2019.04.006

Maàla, K. A. (2008). *Geological map of Sulaimaniya quadrangle sheet NI-38-3, scale 1: 250.000* (1st ed.). Iraq Geological Survey.

Miller Rosen, A. (1986). *Cities of clay, the geoarcheology of tells* (p. 167). University of Chicago Press.

NextGIS. (2021). QuickMapServices. https://nextgis.com/blog/quickmapservices/

Obaid, A. K., & Allen, M. B. (2017). Landscape maturity, fold growth sequence and structural style in the Kirkuk Embayment of the Zagros, northern Iraq. *Tectonophysics*, *717*, 27–40. https://doi.org/10.1016/j.tecto.2017.07.006

Obaid, A. K., & Allen, M. B. (2019). Landscape expressions of tectonics in the Zagros fold-and-thrust belt. *Tectonophysics*, *766*, 20–30. ISSN 0040-1951. https://doi.org/10.1016/j.tecto.2019.05.024

Owen, L. A., & Shroder, J. F. (2013). Tectonic geomorphology. In *Treatise on geomorphology*. Elsevier: Academic Press.

Perego, A., Zerboni, A., & Cremaschi, M. (2011). Geomorphological Map of the Messak Settafet and Mellet (central Sahara, SW Libya). *Journal of Maps*, *7*(1), 464–475. https://doi.org/10.4113/jom.2011.1207

Peyronel, L., Minniti, C., Moscone, D., Naime, Y., Oselini, V., Perego, R., & Vacca, A. (2019). The Italian Archaeological Expedition in the Erbil Plain, Kurdistan Region of Iraq. Preliminary Report on the 2016-2018 Excavations at Helawa. Mesopotamia, Vol. 54, pp. 1–104.

QGIS Development Team. (2021). QGIS Geographic Information System. Open Source Geospatial Foundation Project.

Ramsey, L. A., Walker, T., & Jackson, J. (2008). Fold evolution and drainage development in the Zagros mountains of Fars province, SE Iran. *Basin Research*, *20*(1), 23–48. https://doi.org/10.1111/j.1365-2117.2007.00342.x

Rivas-Martìnez, S. (2004). *Global Bioclimatics (Clasificación Bioclimática de la Tierra)*. Worldwide Bioclimatic Classification System. Phytosociological Research Center. http://www.global-bioclimatics.org

Shamaran Petroleum. (2011). Kurdistan oil & gas activity. Retrieved November, 2011, from http://www.

iraqoilforum.com/wp-content/uploads/2011/11/Kurdistan-Oil-Gas-Activity-Map-Nov-2011.pdf

Siravo, G., Molin, P., Sembroni, A., Fellin, M. G., & Faccenna, C. (2021). Tectonically driven drainage reorganization in the Eastern Cordillera, Colombia. *Geomorphology*, *389*, Article 107847. ISSN 0169-555X. https://doi.org/10.1016/j.geomorph.2021.107847

Sissakian, V. K. (2013). *Geological Map of Kirkuk Quadrangle Sheet NI-38-2, Scale 1: 250.000* (2nd ed.). Iraq Geological Survey.

Sissakian, V. K., Al-Ansari, N., & Abdullah, N. H. (2020). Indicating the possibility of activation of large and old landslides and risk estimation using remote sensing and field data, examples from the Iraqi Kurdistan Region, Iraq. *Geotectonics*, *54*(2), 240–255. ISSN 0016-8521. https://doi.org/10.1134/S0016852120020107

Sissakian, V. K., & Al-Jibouri, B. S. M. (2012). Stratigraphy of the low folded zone. *Iraqi Bull. Geol. Min*, (5), 63–132. Geology of the Low Folded Zone.

Sissakian, V. K., & Al-Jibouri, B. S. M. (2014). Stratigraphy of the high folded zone. *Iraqi Bull. Geol. Min*, (6), 73–161. Geology of the High Folded Zone.

Sissakian, V. K., Al-Mousawi, H. A., Al-Ansari, N., & Knutsson, S. (2015). Old alluvial fan relics in north and northeast Iraq. *Journal of Earth Sciences and Geotechnical Engineering*, *5*(2), 45–62. ISSN: 1792-9040 (print), 1792-9660 (online).

Sissakian, V. K., & Fouad, S. F. (2015). Geological map of Iraq, scale 1: 1000 000, 2012. *Iraqi Bulletin of Geology and Mining*, *11*(1), 9–16.

Sissakian, V. K., & Fouad, S. F. A. (2012). *Geological Map of Iraq, scale 1: 1000000* (4th ed.). Iraq Geological Survey.

Sissakian, V. K., & Fouad, S. F. A. (2014). *Geological Map of arbeel and mahabad quadrangles sheet NJ-38-14 and sheet NJ-38-15, scale 1: 250.000* (2nd ed.). Iraq Geological Survey.

Sissakian, V. K., Ghafur, A. A., Abdulhaq, H. A., & Omer, H. O. (2021). Shakrook anticline, a very complicated structural form, North Iraq, Kurdistan Region. *Iraqi Geological Journal*, *54*(2F), 162–177. https://doi.org/10.46717/igj.54.2F.14ms-2021-12-31

Sissakian, V. K., Kadhim, T. H., & Jab'bar, M. W. A. (2014). Geomorphology of the high folded zone. *Iraqi Bull. Geol. Min*, (6), 7–51. Geology of the High Folded Zone.

Sissakian, V. K., Othman, A. A., & Shihab, A. T. (2018). Factors controlling the development of wine-glass forms in the mountains of the Kurdistan Region, Iraq. *Aro-The Scientific Journal of Koya University*, *6*(2), 39–48. https://doi.org/10.14500/aro.10415

Soroush, M., Mehrtash, A., Khazraee, E., & Ur, J. A. (2020). Deep learning in archaeological remote sensing: Automated Qanat detection in the Kurdistan Region of Iraq. *Remote Sensing*, *12*(3), 500. https://doi.org/10.3390/rs12030500

Strahler, A. N. (1958). Dimensional analysis applied to fluvially eroded landforms. *Geological Society of America Bulletin*, *69*(3), 279–300. https://doi.org/10.1130/0016-7606(1958)69[279:DAATFE]2.0.CO;2

Tooth, S., McCarthy, T., Rodnight, H., Keen-Zebert, A., Rowberry, M., & Brandt, D. (2014). Late Holocene development of a major fluvial discontinuity in floodplain wetlands of the Blood River, eastern South Africa. *Geomorphology*, *205*, 128–141. ISSN 0169-555X. https://doi.org/10.1016/j.geomorph.2011.12.045

Trost, G., Robl, J., Hergarten, S., & Neubauer, F. (2020). The destiny of orogen-parallel streams in the Eastern Alps: The Salzach–Enns drainage system. *Earth Surface Dynamics*, *8*(1), 69–85. https://doi.org/10.5194/esurf-8-69-2020

Tveite, H. (2015). Line direction histogram QGIS plugin [WWW Document]. http://arken.umb.no/~havatv/gis/qgisplugins/LineDirectionHistogram/

Ur, J., Babakr, N., Palermo, R., Creamer, P., Soroush, M., Ramand, S., & Nováček, K. (2021). The Erbil Plain archaeological survey: Preliminary results, 2012–2020. *Iraq*, *83*, 205–243. https://doi.org/10.1017/irq.2021.2

USGS. (1968). Declassified Corona imaging data. Retrieved August 16, 2020, from https://corona.cast.uark.edu

Vergés, J., Saura, E., Casciello, E., Fernàndez, M., Villaseñor, A., Jiménez-Munt, I., & Garcìa-Castellanos, D. (2011). Crustal-scale cross-sections across the NW Zagros belt: Implications for the Arabian margin reconstruction. *Geological Magazine*, *148*(5–6), 739–761. https://doi.org/10.1017/S0016756811000331

Viltres, R., Jónsson, S., Alothman, A., Liu, S., Leroy, S., Masson, F., Doubre, C., & Reilinger, R. (2022). Present-day motion of the Arabian plate. *Tectonics*, *41*(3), e2021TC007013. https://doi.org/10.1029/2021TC007013

Wilkinson, T. J. (2003). *Archaeological landscapes of the near east*. University of Arizona Press.

Woolderink, H. A. G., Cohen, K. M., Kasse, C., Kleinhans, M. G., & Van Balen, R. T. (2021). Patterns in river channel sinuosity of the Meuse, Roer and Rhine rivers in the Lower Rhine Embayment rift-system, are they tectonically forced? *Geomorphology*, *375*, Article 107550. ISSN 0169-555X. https://doi.org/10.1016/j.geomorph.2020.107550

Yacoub, S. Y., Othman, A. A., & Kadhim, T. H. (2012). Geomorphology of the low folded zone. *Iraqi Bull. Geol. Min*, (4), 7–37. Geology of the Low Folded Zone.

Yamazaki, D., Ikeshima, D., Tawatari, R., Yamaguchi, T., O'Loughlin, F., Neal, J. C., Sampson, C. C., Kanae, S., & Bates, P. D. (2017). A high accuracy map of global terrain elevations. *Geophysical Research Letters*, *44*(11), 5844–5853. https://doi.org/10.1002/2017GL072874

Zebari, M., Balling, P., Grutzner, C., Navabpour, P., Witte, J., & Ustaszewski, K. (2020). Structural style of the NW Zagros Mountains and the role of basement thrusting for its Mountain Front Flexure, Kurdistan Region of Iraq. *Journal of Structural Geology*, *141*, Article 104206. ISSN 0191-8141. https://doi.org/10.1016/j.jsg.2020.104206

Zebari, M., Grutzner, C., Navabpour, P., & Ustaszewski, K. (2019). Relative timing of uplift along the Zagros mountain front flexure (Kurdistan Region of Iraq): constrained by geomorphic indices and landscape evolution modeling. *Solid Earth*, *10*(3), 663–682. https://doi.org/10.5194/se-10-663-2019

Zebari, M., Preusser, F., Grutzner, C., Navabpour, P., & Ustaszewski, K. (2021). Late Pleistocene-Holocene slip rates in the northwestern Zagros Mountains (Kurdistan Region of Iraq) derived from luminescence dating of river terraces and structural modeling. *Tectonics*, *40*(8), e2020TC006565. https://doi.org/10.1029/2020TC006565

Zerboni, A., Perego, A., & Cremaschi, M. (2015). Geomorphological map of the tadrart acacus massif and the Erg Uan kasa (Libyan central sahara). *Journal of Maps*, *11*(5), 772–787. https://doi.org/10.1080/17445647.2014.955891

Zerboni, A., Perego, A., Mariani, G. S., Brandolini, F., Al Kindi, M., Regattieri, E., Zanchetta, G., Borgi, F., Charpentier, V., & Cremaschi, M. (2020). Geomorphology of the Jebel Qara and coastal plain of Salalah (Dhofar, southern Sultanate of Oman). *Journal of Maps*, *16*(2), 187–198. https://doi.org/10.1080/17445647.2019.1708488